Appl. Phys. A 81, 1639–1645 (2005)
DOI: 10.1007/s00339-005-3320-3

Applied Physics A
Materials Science & Processing

I.M. BURAKOV[1]
N.M. BULGAKOVA[1,✉]
R. STOIAN[2]
A. ROSENFELD[3]
I.V. HERTEL[3,4]

Theoretical investigations of material modification using temporally shaped femtosecond laser pulses

[1] Institute of Thermophysics SB RAS, 1 Lavrentyev Ave., 630090 Novosibirsk, Russia
[2] Laboratoire TSI (UMR 5516 CNRS), Université Jean Monnet, 10 rue Barrouin, 42000 Saint Etienne, France
[3] Max-Born-Institut für Nichtlineare Optik und Kurzzeitspektroskopie, Max-Born Str. 2a, 12489 Berlin, Germany
[4] Department of Physics, Free University of Berlin, Arnimallee 14, 14195 Berlin, Germany

Received: 3 March 2005/Accepted: 22 June 2005
Published online: 4 August 2005 •

ABSTRACT We present a two-dimensional model, based on a drift–diffusion approach, developed to describe the dynamics of electronic excitation and lattice heating in several dielectric materials with different electron–phonon coupling properties (e.g. fused silica and sapphire) under the action of femtosecond near-infrared laser pulse trains with variable separation time between pulses. The modeling approach was aimed to describe the mechanisms that enable the spatial modulation of the structures induced by temporally modulated laser excitation and ablation of wide-band-gap dielectric materials. The possible geometric contours of the laser-induced craters on the target surfaces are discussed on the basis of the lattice-temperature profiles obtained by modeling. It was found that the observed difference in the crater shapes generated in fused silica and sapphire is conditioned by the difference in dynamics of electron excitation and recombination channels characteristic of these two materials. This effect can be used to convert a given temporal pulse modulation into spatial modulation, opening up new perspectives for material processing in order to obtain desired structure profiles.

PACS 79.20.Ds; 42.62.-b

1 Introduction

Recent progress in producing energetic and reliable femtosecond lasers for material processing gives strong momentum to further development of contemporary pulsed laser technologies. Ultra-short laser pulses have received much attention as a powerful tool for extremely precise processing of almost any kind of material due to remarkable features of the ultra-short laser pulse interaction with matter, such as minimizing laser–plume interaction and reducing the heat-affected zones. Due to rapid energy delivery, material removal is strongly localized with minimal residual damage and requires less energy than what is usually required when using longer laser pulses [1–3]. These advantages of femtosecond laser pulses are even more pronounced in laser processing of dielectric materials because of highly non-linear absorption and reduced heat diffusion as compared to metals, allowing the generation of well-defined microstructures with high quality and reproducibility [4]. Laser ablation of dielectrics proceeds through a whole sequence of physical processes, such as non-linear absorption, non-equilibrium effects related to electronic and vibrational excitations, and avalanche breakdown, giving rise to the generation of dense, overcritical electron–hole plasmas [5]. Due to electron photoemission the surface is effectively charged, resulting in surface-layer disintegration by Coulomb explosion [5–7]. Repetitive irradiation causes defect accumulation, strongly affecting the dynamics of energy deposition [6, 8].

Temporal pulse shaping by Fourier synthesis of spectral components has been demonstrated to be a powerful technique for controlling a variety of physical and chemical systems and offers enhanced possibilities to route specific processes in pre-specified directions [9, 10]. In the particular field of material processing the techniques present some interesting opportunities. Adequate temporal tailoring of ultra-fast laser pulses will deliver energy to the irradiated solid in a sequence synchronized with the characteristic response of the material. When dielectric materials are exposed to modulated laser radiation, the sequential energy delivery may induce a preparation of the surface (i.e. defined electron density and phonon temperature) and associated material softening during the initial steps of excitation, thus changing the energy coupling for the subsequent steps. This may lead to lower stress, cleaner structures, and provides a material-dependent optimization process, with clear benefits especially for brittle materials. Understanding the underlying physics and the interrelation of the processes taking place in dielectrics irradiated by temporally tailored pulses can open additional ways for optimizing and controlling microprocessing technologies. Energy release into the lattice depends on the capability of the materials to transfer electronic excitations into vibrational modes or in transient lattice-localized deformations associated with carrier trapping. That is the reason we have chosen two types of dielectric materials with different characteristics in relation to the electron–phonon coupling strength: fused silica and sapphire. In oxides with strong electron–phonon coupling such as α-quartz (c-SiO_2) or fused silica (a-SiO_2), fast electron trapping associated with the formation of self-trapped excitons is observed with characteristic times of approximately 100 fs [11]. In other oxides like sapphire (α-Al_2O_3) or magnesium oxide (MgO), the electrons survive at the edge of the conduction band for tens of ps. It has been shown [4, 8] that

✉ Fax: +7-3833-308480, E-mail: nbul@itp.nsc.ru

the characteristic electronic and lattice responses can be exploited in irradiation with temporally shaped pulses in order to improve the structuring process. In this paper we present a two-dimensional (2D) model describing the energy absorption and transport in dielectrics under the action of temporally shaped laser pulses, namely multipulse sequences with variable separation. A modeling tool is developed to calculate the spatial details of the induced structures, an important factor in precise laser machining of surfaces [12–16]. It furthermore enables us to predict and verify assumed physical processes occurring in excited dielectrics. The model sheds additional light onto the characteristics of dielectric optical breakdown, taking into account the temporal and spatial evolution of the free-electron density, defect accumulation, the energies of electron and lattice subsystems, and the optical response in the dielectric targets under the action of temporally modulated pulse intensity envelopes. The 2D extension of rather established one-dimensional (1D) numerical approaches to describe dielectric breakdown under ultra-fast laser excitation is motivated by the direct comparison with experimental spatial profiles of laser-induced craters. In spite of the fact that radial transport should not play an important role when compared to the axial dimension, 2D modeling helps in taking into account the spatial intensity distribution across the irradiated region. Additionally, when investigating the modulated spatial profiles, it should be realized that modulations obtained with a simplified 1D approach do not take into account the 2D effect of the electron thermal conductivity, which tends to straighten the bent isothermal lines. The thermal conduction, negligible on the scale of the irradiation spot, may become important during the modulated sequence. As a result, using 1D modeling can lead to overestimating parameter modulations and the latter can be considerably blurred or disappear completely in the more realistic 2D simulations. Besides calculating the 2D electron densities at the end of the laser sequence, the model establishes the spatial profiles of the isotherms. It provides a verification of the fact that electron trapping plays a fundamental role in defining the final spatial profile, based on the potential energy localized at defect sites. Modeling was performed for sapphire and fused silica in order to emphasize the material-dependent energy-deposition time scales (modulated electronic excitation and optimal energy transfer to the lattice) for particular experimental conditions. The temperature profiles obtained by modeling are analyzed and compared with the experimental data on crater shapes. It has been found that developing the antireflective properties is responsible for the formation of the modulated crater in fused silica.

2 The model

The model is based on the one-dimensional (1D) approach proposed in [5] to describe fast electronic transport in different classes of materials (metals, semiconductors, and dielectrics) under ultra-fast, pulsed laser irradiation, and developed to the two-dimensional (2D) case that implies cylindrical symmetry for the problem of laser excitation. 2D features of energy deposition into the lattice or glass matrix, which define the resulting crater shapes, are of primary interest. It has been shown that lattice heating is affected only slightly by the laser-induced electric current [17], so the effects of surface charging and the associated ambipolar electric field are ignored. The modeling is based on solving the equations listed below. The continuity equations for the laser-generated free electrons, holes, and defects take into account the processes of multiphoton ionization, avalanche, and electron recombination:

$$\frac{\partial n_\mathrm{e}}{\partial t} = \left(W_\mathrm{mph} + Q_\mathrm{AV}\right)\frac{n_\mathrm{a}}{n_0} - R_\mathrm{e}\,, \tag{1}$$

$$\frac{\partial n_\mathrm{d}}{\partial t} = R_\mathrm{e}\,, \tag{2}$$

$$n_\mathrm{a} = n_0 - n_\mathrm{e} - n_\mathrm{d}\,. \tag{3}$$

Here, we assume that $n_\mathrm{i} = n_\mathrm{e}$; n_a, n_i, n_e, and n_d are the densities of neutral and ionized atoms, electrons excited to the conduction band, and defects, respectively; $W_\mathrm{mph} = \sigma_6 I^6$ is the rate of a six-photon ionization process corresponding to an energy-forbidden band E_g of approximately 9 eV (for materials under consideration irradiated with 800-nm laser wavelength); n_0 is the total atomic number density of the lattice ($1.17 \times 10^{23}\,\mathrm{cm}^{-3}$ for Al_2O_3 and $6.6 \times 10^{22}\,\mathrm{cm}^{-3}$ for SiO_2); $Q_\mathrm{AV} = \alpha n_\mathrm{e} I$ is the avalanche term [18]; and R_e represents the decay term taken in the form of a relaxation time approximation $n_\mathrm{e}/\tau_\mathrm{tr}$, describing a trapping-like phenomenon (with τ_tr equal to 100 ps for sapphire and 100 fs for fused silica). It has been suggested recently [19] that transient defect population should be taken into account when describing the complex optical response, but the absence of a reliable cross section for defect absorption has been a major impediment in considering this type of response in the present work. We assume that carrier trapping in self-induced lattice deformations is the dominant recombination process. Both multiphoton ionization and avalanche terms are corrected for the reduction in the density of ionization centers (neutral atoms providing the electrons in the valence band) during ionization. The multiphoton ionization cross section σ_6 ($\sigma_6 = 8 \times 10^9\,\mathrm{cm}^{-3}\,\mathrm{ps}^{-1}/(\mathrm{TW/cm}^2)^6$ for sapphire and $\sigma_6 = 6 \times 10^8\,\mathrm{cm}^{-3}\,\mathrm{ps}^{-1}/(\mathrm{TW/cm}^2)^6$ for fused silica) and the avalanche coefficient α ($\alpha = 6\,\mathrm{cm}^2/\mathrm{J}$ for sapphire and $\alpha = 4\,\mathrm{cm}^2/\mathrm{J}$ for fused silica) were estimated based on a fit to the experimental results for the optical damage threshold [20] following a similar approach to [18], taking into account the observed decay in the threshold electron density at longer pulse durations [21].

The laser pulse train consists of a sequence of the laser pulses with the intensity profiles of the Gaussian temporal and spatial form:

$$I(0,r,t) = (1 - R(r,t))\,\frac{2F_0}{\tau_\mathrm{L}}\sqrt{\frac{\ln 2}{\pi}} \times \exp\left[-4\ln 2\left(\frac{t}{\tau_\mathrm{L}}\right)^2\right]\exp\left[-\left(\frac{r}{R_0}\right)^2\right], \tag{4}$$

where F_0 is the incident laser fluence, r is the radial coordinate, $R_0 = 1.5 \times 10^{-5}$ m is the irradiation-spot radius, $\tau_\mathrm{L} = 100$ fs is the laser pulse duration (FWHM), and $R(r,t)$ is the reflection coefficient. We consider a sequence of three identical pulses, although, for more complicated situations, the values of F_0 and τ_L can be arbitrarily chosen and vary from

pulse to pulse. The spatially and temporally dependent laser power inside the dielectric target is determined by loss mechanisms involving free-electron generation and by the optical response of a collisional free-electron plasma as

$$\frac{\partial}{\partial z} I\,(z, r, t) = -W_{\mathrm{mph}} \frac{n_0 - n_{\mathrm{e}}}{n_0} \hbar\omega n_{\mathrm{ph}} - \alpha_{\mathrm{e}}\,(z, r, t)\, I\,(z, r, t)\ , \tag{5}$$

where z is the distance from the target surface toward the bulk depth and n_{ph} is the number of photons for multiphoton ionization ($n_{\mathrm{ph}} = 6$). The optical response of the dielectric target under breakdown conditions is calculated through the complex dielectric function $\varepsilon(n_{\mathrm{e}})$, which can be seen as a mutual contribution of the unexcited solid and the response of the laser-induced free-electron gas [18, 22]:

$$\varepsilon\,(n_{\mathrm{e}}) = 1 + \left(\varepsilon_{\mathrm{g}} - 1\right)\left(1 - \frac{n_{\mathrm{e}}}{n_{0\mathrm{e}}}\right) - \frac{n_{\mathrm{e}}}{n_{\mathrm{cr}}} \frac{1}{1 + \mathrm{i}\frac{1}{\omega\tau}}\ . \tag{6}$$

Here, ε_{g} is the dielectric constant of the unexcited material ($\varepsilon_{\mathrm{g}} = n^2$ with $n = 1.75$ and 1.45 for sapphire and fused silica, respectively [23]); $n_{\mathrm{c}} = \varepsilon_0 m_{\mathrm{e}} \omega^2 / e^2$ is the critical electron density ($1.74 \times 10^{21}\ \mathrm{cm}^{-3}$ at 800-nm wavelength); and $n_{0\mathrm{e}}$ is the density of the valence-band electrons. The damping term $\omega\tau$ was chosen to be equal to 3 in order to match the observed reflectivities of $\sim 70\%$ reported in [24] for supercritical electron densities generated by high-intensity radiation. The absorption coefficient α_{e} is thus determined as

$$\alpha_{\mathrm{e}}(z, r, t) = \frac{2\sqrt{2}\pi}{\lambda} \left(-\mathrm{Re}(\varepsilon) + \sqrt{(\mathrm{Re}(\varepsilon))^2 + (\mathrm{Im}(\varepsilon))^2}\right)^{1/2}\ . \tag{7}$$

We assume that strongly ionized insulators can be considered as dense plasmas and hence the two-temperature model by the analogy with metals [25] can be used to describe the heating of the electron and lattice subsystems [17]:

$$C_{\mathrm{e}} \frac{\partial T_{\mathrm{e}}}{\partial t} = \nabla\,(K_{\mathrm{e}} \nabla T_{\mathrm{e}}) - g\,(T_{\mathrm{e}} - T_{\mathrm{l}}) + S\,(z, r, t)\ , \tag{8}$$

$$C_{\mathrm{l}} \frac{\partial T_{\mathrm{l}}}{\partial t} = g\,(T_{\mathrm{e}} - T_{\mathrm{l}})\ . \tag{9}$$

Here, indices e and l refer to the electron and lattice parameters: C_{e}, C_{l}, and K_{e} are the heat capacities of free electrons and the lattice and the electron thermal conductivity (for ultrashort time scales of the order of 1 ps the lattice thermal conductivity can be neglected); $g = C_{\mathrm{e}}/\tau_{\mathrm{r}}$ is the electron–lattice coupling constant with τ_{r} being the characteristic electron–lattice energy-relaxation time ($\tau_{\mathrm{r}} \sim 1$ ps for both sapphire and fused silica); and $S(z, r, t)$ is the volume energy source term. The source term for the temperature defines the average energy of the particles in the form [17]

$$S(z, r, t) = n_{\mathrm{e}} \frac{\partial E_{\mathrm{e}}}{\partial t} = \frac{\partial E_{\mathrm{f}}}{\partial t} - \frac{3}{2} k T_{\mathrm{e}} \frac{\partial n_{\mathrm{e}}}{\partial t}\ . \tag{10}$$

Here, E_{e} is the average energy per free electron ($E_{\mathrm{e}} = 3\,kT_{\mathrm{e}}/2$) and E_{f} is the total energy of the electronic subsystem. The thermodynamic parameters for the electronic subsystem are taken according to [26]: $C_{\mathrm{e}} = 3\,k_{\mathrm{B}} n_{\mathrm{e}}/2$ and $K_{\mathrm{e}} = 2\,k_{\mathrm{B}}^2 n_{\mathrm{e}} \mu_{\mathrm{e}} T_{\mathrm{e}}/e$, where μ_{e} is the electron mobility ($\mu_{\mathrm{e}} = 3 \times 10^{-5}\ \mathrm{m}^2/(\mathrm{V\,s})$ [27] for sapphire and $2 \times 10^{-4}\ \mathrm{m}^2/(\mathrm{V\,s})$ for fused silica [28], 10 times lower than the reported values, to describe the mobility decrease at high electronic densities). The lattice heat capacity was taken as $C_{\mathrm{l}} = 3\,k_{\mathrm{B}} n_0$.

The dynamics of the total energy of the electronic subsystem is followed in time according to the energy balance, taking into account the processes of multiphoton ionization, avalanche, free-electron absorption, and defect formation [17]:

$$\frac{\partial E_{\mathrm{f}}}{\partial t} = \left(n_{\mathrm{ph}}\hbar\omega - E_{\mathrm{g}}\right) W_{\mathrm{mph}} - E_{\mathrm{g}} Q_{\mathrm{AV}} \frac{n_{\mathrm{a}}}{n_0} + \alpha_{\mathrm{e}} I\,(z, r, t) - E_{\mathrm{e}} \frac{n_{\mathrm{e}}}{\tau_{\mathrm{tr}}}\ . \tag{11}$$

The energy-balance equation for defects is

$$\frac{\partial E_{\mathrm{d}}}{\partial t} = E_{\mathrm{e}} \frac{n_{\mathrm{e}}}{\tau_{\mathrm{tr}}}\ , \tag{12}$$

where E_{d} is the total energy stored in defects.

The system of equations (1)–(12) was solved numerically using the explicit numerical scheme written for the 2D case implying cylindrical symmetry. We use an irregular grid that provides good accuracy and a large numerical region, requiring therewith a reasonable computer time. The depth of the numerical region was chosen in such a way that a further increase did not influence the numerical results. In both the remote boundary (bulk) with respect to the target surface and the remote transversal boundary with respect to the center of the irradiated spot, the conditions of free in- and out-flow for heat transfer were set, while at the surface–vacuum interface the condition of zero heat exchange was used. All the results given below have been obtained for sapphire and fused silica irradiated by the sequence of three identical laser pulses of 800-nm wavelength with 100-fs duration, total laser fluence of $14\ \mathrm{J/cm}^2$, and variable separation time between pulses.

3 Results and discussion

In the modeling approach we aimed at describing the specific experimental conditions [8] where the possibility of modulating the spatial depth profile as a function of the pulse separation in the excitation sequence was demonstrated. The experimental results are shown in Fig. 1 for a single multipulse excitation sequence per site with different separation times between pulses. No modulation is observed in fused silica with short separation (Fig. 1a, left), whereas increased temporal distances between pulses result in a tendency toward a step profile (Fig. 1a, right). This effect allows converting a temporal pulse modulation into spatial modulation, opening up possibilities to design the desired profiles. Similar irradiation of a sapphire surface has produced no modulation (Fig. 1b). It has been supposed [8] that carrier trapping is responsible for the observed difference in the crater shapes produced in these two materials.

The results of modeling are shown in Figs. 2–5. Figure 2 presents the contour maps of the lattice temperature in sapphire (a) and fused silica (b) generated after the action of

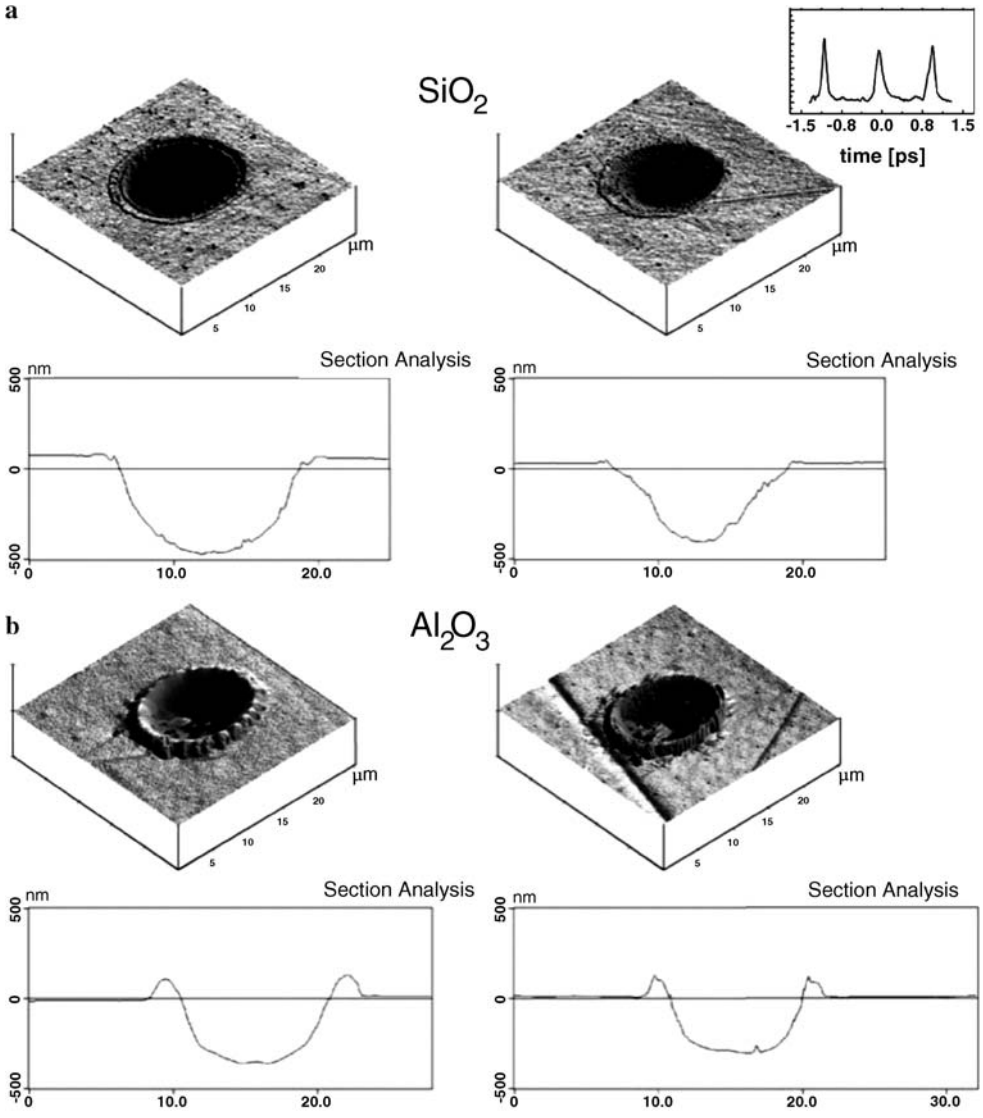

FIGURE 1 (**a**) Single-shot structures made on a-SiO_2 surfaces with triple pulse trains with different separation times at 14 J/cm^2. Reproduced from [8]. *Left*: 0.3-ps separation. *Right*: 1-ps separation. Increasing the temporal distance between the pulses leads to a modulation of the spatial profile. (**b**) Same for Al_2O_3, at 12 J/cm^2 where no spatial modulation is observed

a triple laser pulse with a separation between pulses of 1 ps (the time is counted from the maximum of the first pulse in the sequence). The contour lines of the lattice temperature in the sapphire sample have a smooth oval form (Fig. 2a). In fused silica (Fig. 2b) a certain modulation of the temperature contour lines is developed with a hollow in the center of the irradiation spot, evidently having common features with the crater form observed in the experiments (Fig. 1a, right). This modulation is even more pronounced in Fig. 3a, where the energy of the defects is added to the lattice temperature in fused silica presenting the energy per atom $T_{\rm tot}$ accumulated in the lattice:

$$T_{\rm tot} = T_{\rm l} + E_{\rm d}/(3kn_0)\,. \tag{13}$$

Figure 3b demonstrates that the defect addition to the lattice temperature $T_{\rm d} = E_{\rm d}/(3\,kn_0)$ significantly influences the modulation in fused silica. It must be underlined that in sapphire the number of the generated defects is insignificant on a time scale of several picoseconds, so that their energy does not change noticeably the contour map of the lattice temperature given in Fig. 2a. Moreover, the temperature contour map in sapphire depends marginally on the separation time between pulses. In modeling with a smaller time separation between pulses on the order of several hundred femtoseconds, the geometry of the contour lines for both materials was similar to that shown in Fig. 2a without signs of spatial modulation (for fused silica, the contour map of the lattice temperature after the action of a triple laser pulse with a separation between pulses of 0.3 ps is given in Fig. 4).

Since most of the material is removed following a phase transition, temperature contour lines should be used as a criterion to evaluate the crater geometry. A certain part of the excited material in a surface target layer situated in the middle of the irradiation spot (Fig. 2) is evidently heated above the thermodynamic critical temperature ($T_{\rm c}$). To evaluate $T_{\rm c}$, one can use one of the methods discussed in [29]. For the majority of the materials, an expected value of $T_{\rm c}$ is 1.5–2 times higher than the boiling temperature under atmospheric pressure, which is 2270 K for SiO_2 and 3250 K for Al_2O_3 [30]. So,

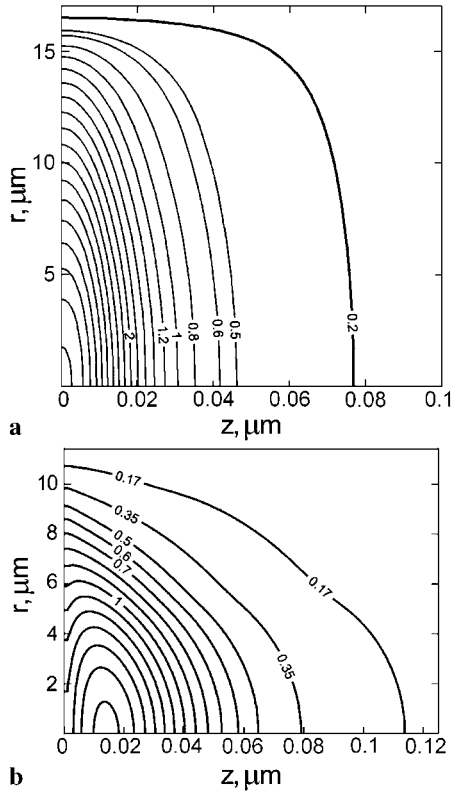

FIGURE 2 Simulated lattice-temperature contour maps obtained for Al_2O_3 (**a**) and a-SiO_2 (**b**) samples after the action of a triple train of identical pulses (1-ps separation) with 100-fs duration and a total fluence of 14 J/cm^2 at 3 ps after the maximum of the first pulse. The temperature levels are marked in eV

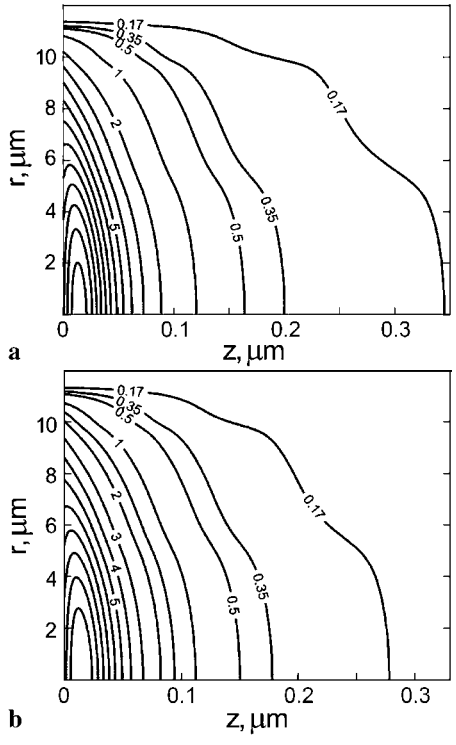

FIGURE 3 Simulation results obtained for fused silica. Laser-irradiation regime is as in Fig. 2. 3 ps after the maximum of the first pulse. (**a**) The contour map of total lattice energy in temperature units taking into account the energy accumulated in defect sites. (**b**) The energy of defects falling on a lattice atom. The contour-map levels are marked in eV

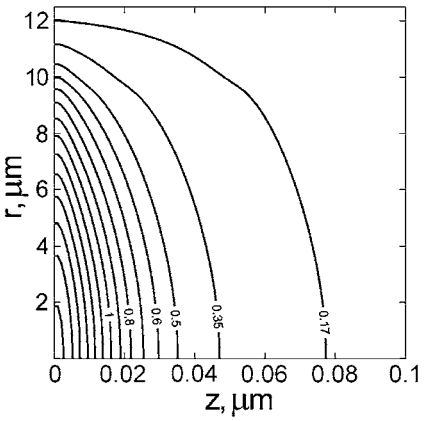

FIGURE 4 Simulated lattice-temperature contour map obtained for fused silica after the action of a triple train of identical pulses with 100-fs duration and 300-fs separation time at 3 ps after the maximum of the first pulse. Total fluence is 14 J/cm^2

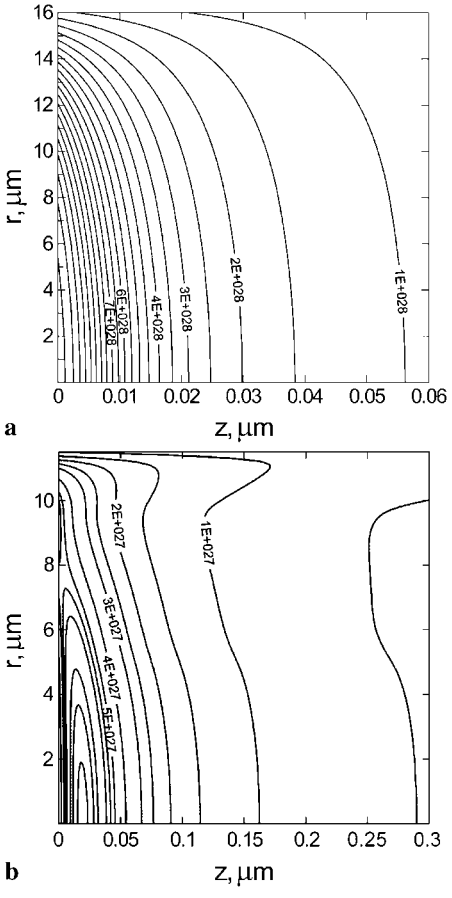

FIGURE 5 Electron-density contour maps for Al_2O_3 (**a**) and a-SiO_2 (**b**) samples for the same irradiation conditions as in Fig. 2 at 2.2 ps after the maximum of the first pulse. The contour-map levels are marked in m^{-3}

the expected value of T_c is around 4000 K for fused silica and between 5000 and 6000 K for sapphire. According to thermodynamic concepts [29, 31, 32], liquid matter rapidly heated close to T_c experiences strong superheating and decays into vapor and liquid droplets through explosive boiling (phase explosion). Moreover, in extremely fast processes like ultrashort laser ablation, the superheated fluid matter can cross the spinodal line and decay into the gas phase without the for-

mation of the critical vapor nuclei [33, 34]. As a rough guide, a liquid zone with a temperature above T_c should be ablated through spinodal decomposition, forming a crater shape corresponding to a 'critical' contour of the lattice temperature, ~ 0.5 eV for sapphire and ~ 0.35 eV for fused silica (Fig. 2). A brief comparison of Figs. 1 and 2 shows that the corresponding 'critical' contours are in good qualitative agreement with the experimental data on crater geometries.

From the thermodynamic point of view, the following effect observed in the experiments [8] can also be understood. Irradiation of sapphire samples produces smeared features due to solidified melt splashed from the crater, while the borders of the craters in fused silica are rather clean (see Fig. 1). Although the melting temperatures T_m of these two materials differ little (2006 K for SiO_2 [35] and 2320 K for Al_2O_3 [30] (see the outermost lines in Fig. 2)) as compared to the difference in the boiling temperatures, the melting processes proceed differently. In sapphire, melting is a first-order phase transition, the process being accompanied by a discontinuous change in the material properties. This implies that the liquid and solid states are separated by a region of a final size where the material is heated to the melting temperature and absorption of the fusion heat takes place. In fused silica, melting is a second-order phase transition that means that there is no discontinuous change in the properties (e.g. in density and viscosity) and no latent heat of fusion. The viscosity of a glass decreases gradually with heating, while molten sapphire has a low viscosity so that it is very sensitive to a minor perturbation [36]. Under spinodal decomposition, vapor particles have extremely high kinetic energies [34] and their recoil pressure forces the melt to come out of the crater, forming a rim on its edge [35, 37]. The higher the value of T_c, the higher the particle kinetic energy and the greater the recoil pressure. The greater the recoil pressure and the thicker the melt layer, the more melt is splashed from the crater, as in the case of sapphire (see Fig. 2a, where the melt zone is located between the two outermost lines with T_m and T_c). As for fused silica, during the melting process the defect energy is released to the lattice ensuring strong superheating of the matter with the temperature above the melting point and, hence, significantly reducing the width of the melt zone (compare Figs. 2b and 3).

It should be noted that other factors should also be taken into account in such analysis, for example surface quality, surface tension, and thermal conductivity influencing strongly the solidification process. However, the behavior of the thermodynamic parameters of specific substances at high temperatures is still an open question. According to the dynamic scaling theory [38], the parameters have no time to relax to their equilibrium values in fast processes like fs laser ablation, and we restrict our modeling and discussion to the results obtained with the parameters known from the literature.

What are the factors that intervene in the crater spatial modulation? The answer becomes evident from Fig. 5 where the contour maps of the free-electron density are presented for the cases shown in Fig. 2. In the sapphire sample (Fig. 5a), due to slow trapping dynamics, the maximum of the free-electron density generated in the course of the pulse sequence action is located on the target surface in the middle of the irradiation spot, leading to enhanced laser energy absorption in this region and, correspondingly, to increased lattice heating. One can see an obvious conformity of the contour maps of the temperature and the free-electron density (Figs. 2 a and 5a). In fused silica (Fig. 5b), the contour map of the free-electron density is more complicated. Because of the rapid trapping process, the surface layer in the middle of the irradiation spot is depleted of free electrons, so that the maximum of the free-electron density is shifted toward the bulk and toward the irradiation-spot periphery. The formation of a ring of the free-electron density in the surface layer with its maximum located in the irradiation-spot periphery is remarkable. Hence, modulation of the free electron density distribution and the associated laser energy absorption results in modulation of lattice heating and ablation.

4 Conclusions

We have presented a 2D model describing the dynamics of electronic excitation, defect formation, and lattice heating in dielectrics under irradiation by a temporally modulated femtosecond laser pulse. Laser-induced heating of the sapphire and fused-silica samples was analyzed and the temperature-contour plots are compared with the crater geometries observed in experiments. It is demonstrated that the material-characteristic relaxation time can have an important influence in establishing the limits of the excitation regions and the range of influence for temporally modulated pulses. If the relaxation time is considerably higher than the laser modulation time, as in the case of sapphire, the material is basically insensitive to the temporal details of the laser excitation. The situation is reversed for materials with high electron–phonon coupling and the transient optical properties are defined to a certain extent by the fast electronic dynamics. Although the model requires further development concerning mainly the dynamics of the defect states, their re-excitation during the prolonged irradiation sequence, and recombination, it made it possible to clarify the origin of the crater-geometry modulation observed experimentally.

ACKNOWLEDGEMENTS Die Wissenschaftlich-Technologische Zusammenarbeit (WTZ-project RUS01/224), die Deutsche Forschungsgemeinschaft (DFG-project Ro 2074/5-1), the International Science and Technology Center (Grant No. 2310) and the INTAS (Grant No. 03-51-5208) are gratefully acknowledged. In addition, I.M.B. and N.M.B. were supported through funding from the Russian Foundation for Basic Research (Project No. 05-02-16170).

REFERENCES

1 B.N. Chichkov, C. Momma, S. Nolte, F. von Alvensleben, A. Tünnermann: Appl. Phys. A **63**, 109 (1996)
2 H. Varel, D. Ashkenasi, A. Rosenfeld, R. Herrmann, F. Noack, E.E.B. Campbell: Appl. Phys. A **62**, 293 (1996)
3 J. Meijer, K. Du, A. Gillner, D. Hoffmann, V.S. Kovalenko, T. Masuzawa, A. Ostendorf, R. Poprawe, W. Schulz: Ann. CIRP **51**, 531 (2002)
4 R. Stoian, M. Boyle, A. Thoss, A. Rosenfeld, G. Korn, I.V. Hertel, E.E.B. Campbell: Appl. Phys. Lett. **80**, 353 (2002)
5 N.M. Bulgakova, R. Stoian, A. Rosenfeld, I.V. Hertel, E.E.B. Campbell: Phys. Rev. B **69**, 054 102 (2004)
6 R. Stoian, D. Ashkenasi, A. Rosenfeld, E.E.B. Campbell: Phys. Rev. B **62**, 13 167 (2000)
7 R. Stoian, A. Rosenfeld, D. Ashkenasi, I.V. Hertel, N.M. Bulgakova, E.E.B. Campbell: Phys. Rev. Lett. **88**, 097 603 (2002)
8 R. Stoian, M. Boyle, A. Thoss, A. Rosenfeld, G. Korn, I.V. Hertel: Appl. Phys. A **77**, 265 (2003)

9 D. Meshulach, Y. Silberberg: Nature **396**, 239 (1998)
10 A. Assion, T. Baumert, M. Bergt, T. Brixner, B. Kiefer, V. Seyfried, M. Strehle, G. Gerber: Science **282**, 919 (1998)
11 G. Petite, P. Daguzan, S. Guizard, P. Martin: Nucl. Instrum. Methods Phys. Res. B **107**, 97 (1996)
12 S. Guizard, A. Semerok, J. Gaudin, M. Hashida, P. Martin, F. Quéré: Appl. Surf. Sci. **186**, 364 (2002)
13 T.Q. Jia, Z.Z. Xu, R.X. Li, D.H. Feng, X.X. Li, C.F. Cheng, H.Y. Sun, N.S. Xu, H.Z. Wang: J. Appl. Phys. **95**, 5166 (2004)
14 L. Jiang, H.L. Tsai: J. Phys. D: Appl. Phys. **37**, 1492 (2004)
15 L. Jiang, H.L. Tsai: Int. J. Heat Mass Transfer **48**, 487 (2005)
16 T.E. Itina, M. Mamatkulov, M. Sentis: Opt. Eng. **44**, 051 109 (2005)
17 N.M. Bulgakova, R. Stoian, A. Rosenfeld, W. Marine, E.E.B. Campbell: Proc. SPIE **5448**, 121 (2004)
18 B.C. Stuart, M.D. Feit, S. Herman, A.M. Rubenchik, B.W. Shore, M.D. Perry: Phys. Rev. B **53**, 1749 (1996)
19 S.S. Mao, F. Quéré, S. Guizard, X. Mao, R.E. Russo, G. Petite, P. Martin: Appl. Phys. A **79**, 1695 (2004)
20 D. Ashkenasi, R. Stoian, A. Rosenfeld: Appl. Surf. Sci. **154–155**, 40 (2000)
21 F. Quèrè, S. Guizard, P. Martin, G. Petite, O. Gobert, P. Meynadier, M. Perdrix: Appl. Phys. B **68**, 459 (1999)
22 K. Sokolowski-Tinten, D. von der Linde: Phys. Rev. B **61**, 2643 (2000)
23 W.G. Driscoll, W. Vaughan (Eds): *Handbook of Optics* (McGraw-Hill, New York 1978)
24 D. von der Linde, H. Schüler: J. Opt. Soc. Am. B **13**, 216 (1996)
25 S.S. Wellershoff, J. Hohlfeld, J. Güdde, E. Matthias: Appl. Phys. A **69**, 99 (1999)
26 H.M. van Driel: Phys. Rev. B **35**, 8166 (1987)
27 R.C. Hughes: Phys. Rev. B **19**, 5318 (1979)
28 R.C. Hughes: Phys. Rev. Lett. **30**, 1333 (1973)
29 N.M. Bulgakova, A.V. Bulgakov: Appl. Phys. A **73**, 199 (2001)
30 I.S. Grigoryev, E.Z. Meilikhov, A.A. Radzig (Eds): *Handbook of Physical Quantities* (CRC, Boca Raton, FL 1995)
31 V.P. Skripov: *Metastable Liquids* (Halsted, New York 1974)
32 N.M. Bulgakova, I.M. Bourakov: Appl. Surf. Sci. **197–198**, 41 (2002)
33 Ya.B. Zeldovich, O.M. Todes: Zh. Eksp. Teor. Fiz. **10**, 1441 (1940) (in Russian)
34 M.M. Martynyuk, N.Yu. Kravchenko: Prikl. Fiz. **1**, 79 (2003) (in Russian)
35 J. Siegel, K. Ettrich, E. Welsch, E. Matthias: Appl. Phys. A **64**, 213 (1997)
36 R.K. Nubling, J.A. Harrington: Appl. Opt. **36**, 5934 (1997)
37 C. Körner, R. Mayerhofer, M. Hartmann, H.W. Bergmann: Appl. Phys. A **63**, 123 (1996)
38 M.A. Anisimov: *Critical Phenomena in Liquids and Liquid Crystals* (Nauka, Moscow 1987) (in Russian)